

A structural study of cyanotrichite from Dachang by conventional and automated electron diffraction

Gennaro Ventrucci¹ · Enrico Mugnaioli^{2,3} · Giancarlo Capitani⁴ · Fernando Scordari¹ · Daniela Pinto¹ · Andrea Lausi⁵

Received: 25 January 2015 / Accepted: 26 April 2015 / Published online: 14 May 2015
© Springer-Verlag Berlin Heidelberg 2015

Abstract The crystal structure of cyanotrichite, having general formula $\text{Cu}_4\text{Al}_2(\text{SO}_4)(\text{OH})_{12}\cdot 2\text{H}_2\text{O}$, from the Dachang deposit (China) was studied by means of conventional transmission electron microscopy, automated electron diffraction tomography (ADT) and synchrotron X-ray powder diffraction (XRPD). ADT revealed the presence of two different cyanotrichite-like phases. The same phases were also recognized in the XRPD pattern, allowing the perfect indexing of all peaks leading, after refinement to the following cell parameters: (1) $a = 12.417(2)$ Å, $b = 2.907(1)$ Å, $c = 10.157(1)$ Å and $\beta = 98.12(1)$; (2) $a = 12.660(2)$ Å, $b = 2.897(1)$ Å, $c = 10.162(1)$ Å and $\beta = 92.42(1)^\circ$. Only for the former phase, labeled cyanotrichite-98, a partial structure, corresponding to the $[\text{Cu}_4\text{Al}_2(\text{OH})_{12}^{2+}]$ cluster, was obtained ab initio by direct methods in space group $C2/m$ on the basis of electron diffraction data. Geometric and charge-balance considerations allowed to reach the whole structure model for the cyanotrichite-98 phase. The sulfate group and water molecule result to be statistically disordered over two

possible positions, but keeping the average structure consistent with the C -centering symmetry, in agreement with ADT results.

Keywords Cyanotrichite · Powder X-ray diffraction · Precession electron diffraction (PED) · Automated electron diffraction tomography (ADT)

Introduction

Cyanotrichite is a hydrated, hydroxylated copper aluminum sulfate, first recognized as new mineral species by Werner (1808). The accepted stoichiometry, according to Palache et al. (1951), is $\text{Cu}_4\text{Al}_2\text{SO}_4(\text{OH})_{12}\cdot 2\text{H}_2\text{O}$. In the past, it was also known under the name lett-somite (Percy 1850) and namaqualite (Mason 1961). It is a member of the cyanotrichite group, which includes cyanotrichite, carbonate-cyanotrichite $\text{Cu}_4\text{Al}_2(\text{CO}_3, \text{SO}_4)(\text{OH})_{12}\cdot 2\text{H}_2\text{O}$ (Ankinovich et al. 1963), camerolaite $\text{Cu}_4\text{Al}_2[\text{HSbO}_4, \text{SO}_4](\text{OH})_{10}(\text{CO}_3)\cdot 2\text{H}_2\text{O}$ and khaidarkanite $\text{Cu}_4\text{Al}_3(\text{OH})_{14}\text{F}_3\cdot 2\text{H}_2\text{O}$ (Rastsvetaeva et al. 1997).

Khaidarkanite and cyanotrichite show very similar unit cell dimensions and are also very similar macroscopically (Hager et al. 2009). Cyanotrichite usually occurs in centimeter to submillimeter sized sky blue clumps or aggregates of fibrous crystals. It represents an oxidation product of copper-bearing deposits subject to weathering in presence of sulfate and aluminum-bearing fluids. It is thus very commonly found associated with other copper minerals such as brochantite, azzurrite and malachite.

Crystallographic data for cyanotrichite are limited. The first powder X-ray diffraction data recorded in the ICDD-PDF database (card. No. 11-0131) were indexed, although not completely, on the basis of an orthorhombic cell with

✉ Gennaro Ventrucci
gennaro.ventrucci@uniba.it

¹ Dipartimento di Scienze della Terra e Geoambientali, Università di Bari, Via Orabona 4, 70125 Bari, Italy

² Dipartimento di Scienze Fisiche, della Terra e dell' Ambiente, Università degli Studi di Siena, Via Laterano 8, 53100 Siena, Italy

³ Institut für Physikalische Chemie, Johannes Gutenberg Universität, Jakob-Welder-Weg 11, 55099 Mainz, Germany

⁴ Dipartimento di Scienze dell' Ambiente e del Territorio e di Scienze della Terra, Università degli Studi di Milano-Bicocca, Milan, Italy

⁵ Sincrotrone Trieste, Strada Statale 14, km 163.5, 34012 Basovizza, TS, Italy

$a = 10.16$, $b = 12.61$, $c = 2.90$ Å. Recently, Walenta (2001), analyzing another cyanotrichite-like phase, suggested that cyanotrichite could be monoclinic. Accordingly, Hager et al. (2009), on the basis of a careful examination of powder patterns, proposed a monoclinic cell with $a = 10.18$, $b = 2.90$, $c = 12.65$ Å, $\beta = 92.5^\circ$. Moreover, they suggested the space group $P2/m$ and inferred some structural features on the basis of the similarity with the khaidarkanite studied by Rastsvetaeva et al. (1997).

Peaks overlapping due to the presence of impurities (e.g., chalcoalumite and brochantite) and/or the admixing of variable amounts of carbonate-cyanotrichite with cyanotrichite is a serious problem for any attempt to solve ab initio the structure of cyanotrichite from powder X-ray diffraction data. Other difficulties arise from the preferred orientation of the acicular-shaped crystallites and the hkl -dependent reflection broadening due to the crystal size effect. On the other hand, cyanotrichite crystals are generally formed by the intergrowth of parallel fibers at the submicrometric scale, which hampers conventional single-crystal X-ray analysis.

Aware of these difficulties, here we have considered the employment of electron diffraction from nanosized volumes. Indeed, the stronger electron–matter interaction, as compared to X-rays, allows to obtain single-crystal electron diffraction data from a very tiny crystallite. On the other hand, the strong electron–matter interaction results in multiple diffraction events that cause the violation of the kinematic assumption that I_{hkl} is proportional to $|F_{hkl}|^2$, a limitation that has restricted the use of electron diffraction for structure solution in the past. Recently, a new approach for electron crystallography, based on the combination of automated diffraction tomography (ADT) (Kolb et al. 2007, 2008) and precession electron diffraction (PED) (Vincent and Midgley 1994), has made possible the collection of more complete 3D electron diffraction data and at the same time to reduce significantly dynamical effects (Mugnaioli et al. 2009a; Kolb et al. 2011). The resulting data proved to be suitable for ab initio structure analysis also for relatively complicated mineral phases (Rozhdestvenskaya et al. 2010, 2011; Gemmi et al. 2011; Mugnaioli et al. 2012; Capitani et al. 2014). Moreover, the use of scanning transmission electron microscopy (STEM) mode for sample recognition and centering reduces the electron dose rate to the sample, allowing the study of electron beam-sensitive materials, such as organic or hydrated inorganic phases (Kolb et al. 2010; Mugnaioli and Kolb 2013). The stability of the target can be further improved using a cryo-holder able to keep the sample at the liquid N₂ temperature (Jiang et al. 2011). In this paper, we report about a TEM and XRPD investigation of cyanotrichite. We found that in the studied samples, two cyanotrichite-like phases are systematically intergrown. One of them was partially solved ab initio using ADT/PED data from individual nanosized domains. The

remaining structure, namely the positions of the missing water molecule and the SO₄²⁻ anion, was deduced via geometric and charge-balance considerations.

Sample and methods

The sample of cyanotrichite investigated in this study comes from the Dachang deposit (Guizhou, China). Preliminary investigation, aiming to check the crystal morphology and composition, was performed by means of semiquantitative energy-dispersive X-ray spectroscopy (EDS) using an Oxford EVO50 scanning electron microscope (SEM) at the University of Bari. Selected crystal fragments were dispersed on an aluminum stub without any carbon coating and analyzed by SEM–EDS under low-vacuum conditions.

Wave-dispersive electron microprobe analyses were carried out with a Jeol 8200 at the Dipartimento di Scienze della Terra of the University of Milan on selected crystallites embedded in epoxy resin and polished. The working conditions were 15 kV accelerating voltage, 2 nA beam current and a 10- μ m beam-spot size. Ten point analyses on as much different crystals were performed. The following standards were employed: Al₂O₃, celestine, Cu metallic, Zn metallic and Co metallic.

Powder Fourier transform infrared (FTIR) spectra were collected on a Nicolet spectrometer equipped with a DTGS detector and a KBr beamsplitter, adopting the KBr pellets technique (1 mg sample per 150 mg KBr). The nominal resolution was 4 cm⁻¹; 128 scans were averaged for both sample and background.

Powder diffraction data were performed at MCX beamline at the “Elettra” Synchrotron, Trieste (Italy), using a diffractometer working in the Debye–Scherrer geometry (Lausi et al. 2006). Data were collected up to 70° (2 θ) using monochromatic radiation ($\lambda = 1.00046$ Å). The sample was fine grounded and loaded within a 0.3-mm silica glass capillary and kept spinning during the data collection. A Le Bail refinement was performed with the General Structure Analysis System (GSAS) program (Larson and Von Dreele 2000). The refinement parameters included the lattice parameters and the Chebyshev background terms. Peak profiles were modeled with a pseudo-Voigt function.

Conventional TEM observations were conducted at the University of Milan with a FEI 20F operated at 200 keV and equipped with an energy-dispersive (EDS) detector, a double-tilt sample holder and a Gatan 794 slow scan CCD camera. A small amount of cyanotrichite fibers was dispersed in ethanol and ultrasonicated. TEM mounts were then prepared by directly placing few drops of the solution onto holey-carbon membranes supported either by copper or gold grids. The latter were used to gather compositional information at the TEM–EDS level.

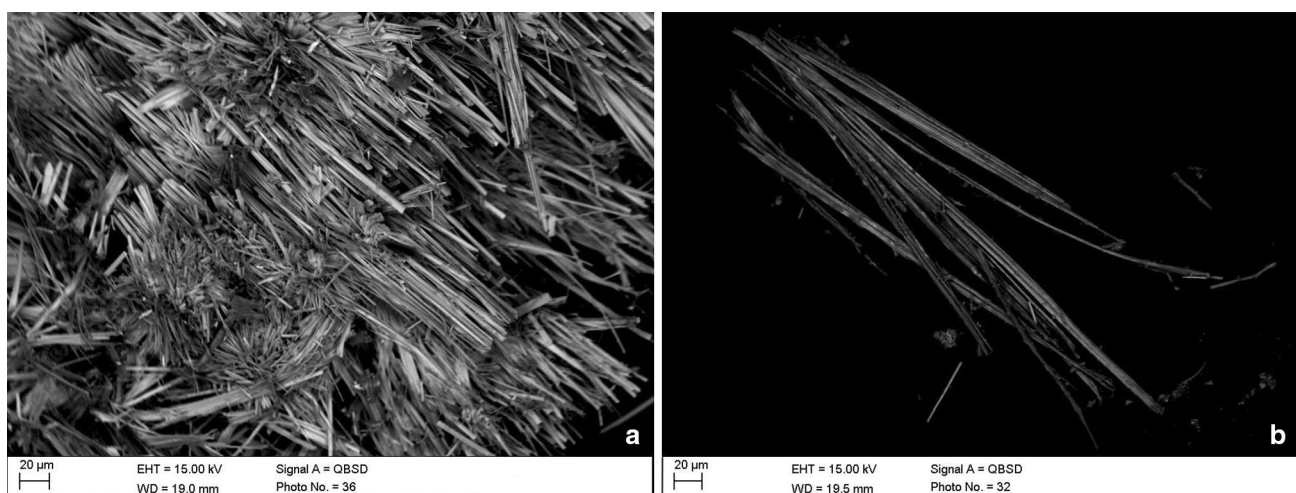


Fig. 1 SEM images of cyanotrichite from Dachang deposit (Guizhou, China). **a** Massive and radiating aggregates of needle-like crystals of cyanotrichite; **b** cyanotrichite crystals formed by the intimate parallel association of thin fibers

Electron diffraction data were obtained combining automated electron diffraction tomography and PED on the same TEM samples. Data collection was performed at the University of Mainz with a Tecnai F30 S-Twin TEM equipped with an emission field gun and operating at 300 kV. Both a Fischione tomography holder (tilt range $\pm 60^\circ$) and a Gatan cryo-holder (tilt range $\pm 45^\circ$) were used. While acquiring a dataset at 155 K temperature, two cryo-traps were used in order to improve and stabilize the vacuum in the TEM column. The ADT tilt series were collected in STEM mode in 1° steps with total tilt ranging from 65 to 100° (eventually limited by other crystal overlapping and crystal degradation under the electron beam). PED was performed using a SpinningStar module (NANO-MEGAS 2004) with a precession angle of 1.2° . ADT data collection was carried out in areas of about 200×200 nm.

Data were processed by the ADT3D package able to perform 3D diffraction reconstruction, automatic unit-cell parameter determination, reflection indexing and intensity integration. *Ab initio* structure solution was accomplished by the direct methods implemented in the SIR2011 software (Burla et al. 2012). Least-squares refinement of the structural model was performed using the SHELXL97 software (Sheldrick 1997). Electron scattering factors were taken from Doyle and Turner (1968).

Results and Discussion

Crystal morphology and microstructure

Cyanotrichite occurs as radiating fibrous aggregates or massive aggregates of tiny, slender, needle-shaped crystals (Fig. 1a). High-magnification SEM images show that

individual cyanotrichite needles do not consist of single crystals but are actually formed by the intimate parallel association of thin fibers (Fig. 1b). In massive samples, the cyanotrichite crystals are often intergrown with other Cu/Al/sulfate and Cu/sulfate crystals, identified by SEM-EDS as chalcocyanite and brochantite, respectively.

Conventional TEM investigations were conducted on several cyanotrichite crystals. Bright-field (BF) images show that parallel needle-like aggregates of cyanotrichite are characterized by an inhomogeneous contrast, due to wafer-thin intergrowths, mineral parting and planar defects (Fig. 2a). This probably accounts for the difficulties encountered so far in the structural analyses and the lack of single-crystal studies. A thoughtful observation of BF images and related selected area electron diffraction (SAED) patterns reveals that, contrary to what assumed from SEM images at the microscopic scale, cyanotrichite possesses a ribbon-like habit rather than acicular. This is inferred from the SAEDs that show always the same orientation to the incident beam, even without significant rearrangement of the tilts. This is possible only if the crystal is flattened parallel to the supporting grid and the thickness along the observation direction is minimal, so that the diffraction rods are very elongated in the beam direction, miming a crystal almost perfectly aligned (Fig. 2b). The diffraction patterns show systematically *Cmm2* symmetry and could be perfectly indexed with a *C*-centered cell, leading to the following 2D cell parameters $a = 12.38(25)$, $b = 2.93(5)$ and $\gamma = 89.8(5)$. These results are in good agreement with the refined XRPD parameters ($a \sim 12.42$, $b \sim 2.91$ Å, $\gamma = 90^\circ$), even considering the distortion usually affecting TEM measurements (e.g., Capitani et al. 2006; Mugnaioli et al. 2009b).

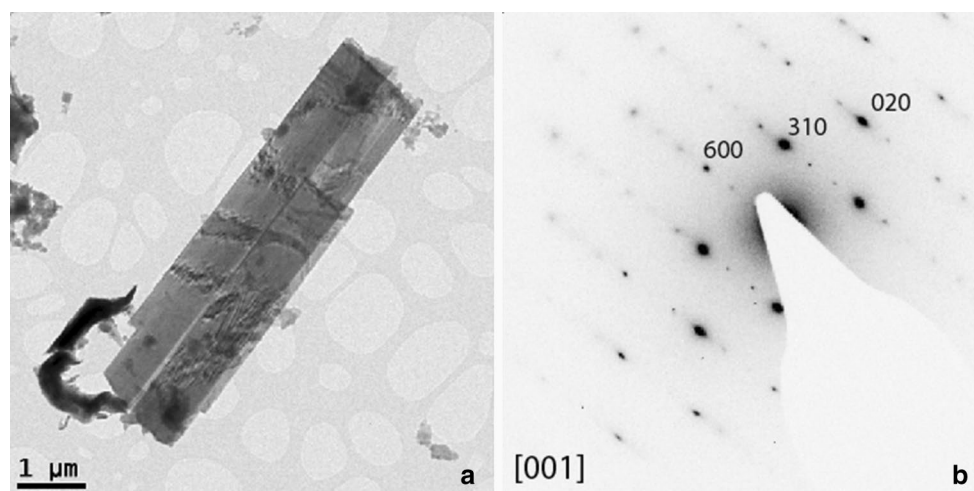


Fig. 2 Bright-field image of cyanotrichite crystals (**a**) and related selected area diffraction pattern (**b**). $hk0$ reflections are present for $h + k = \text{even}$, according to the C -centered cell. Crystals are flattened on (001) and elongated along **b**

Table 1 WDS microprobe results of the studied cyanotrichite sample (1) as compared with the calculated composition and literature data

	Calculated	1	2	3	4	5	6
MgO	–	–	–	0.00	0.10	0.26	0.07
CaO	–	–	0.11	–	0.80	0.55	–
PbO	–	–	–	–	0.29	–	–
ZnO	–	0.17(12)	–	–	1.71	0.62	0.65
CuO	49.38	45.53(71)	47.50	48.30	46.86	44.40	46.48
V ₂ O ₄	–	–	–	–	–	0.16	0.17
Al ₂ O ₃	15.82	17.96(97)	15.59	15.69	16.70	18.10	18.95
SO ₃	12.43	11.67(34)	12.19	12.25	11.80	4.05	4.46
Co ₂ O ₃	–	0.02(4)	–	–	–	–	–
CO ₂	–	–	–	–	–	5.20	4.77
SiO ₂	–	–	–	–	–	2.98	–
P ₂ O ₃	–	–	–	–	0.06	–	–
As ₂ O ₅	–	–	–	–	0.76	–	–
Fe ₂ O ₃	–	–	0.43	–	–	–	–
H ₂ O	22.37	22.58 ^a	23.20	22.05	18.80	22.90	23.97

Sample locality: (1) Dachang, China (this work); (2) Grandview mine, California (Palache et al. 1951); (3) Berkara, Kazakhstan; (4) Lachin, Khana (Uzbekistan); (5) Balasauskandyk, Kazakhstan; (6) Karatau, Kazakhstan (3–6, Ankinovich et al. 1963)

^a Calculated

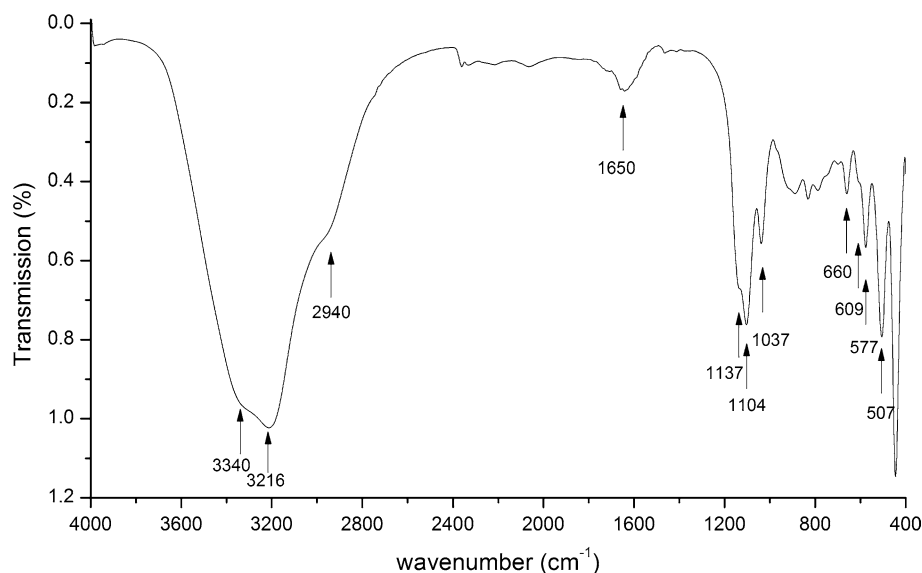
Chemical composition and FTIR results

The analytical results of the investigated cyanotrichite sample by WDS microanalyses are reported in Table 1. No direct determination of H₂O by gravimetric methods was performed owing to the low amount of available sample. The crystals analyzed show a composition similar to the calculated one, although there is a slightly higher Al/Cu ratio. Small variations of the Cu²⁺:Al³⁺:OH[−] proportions are probably due to differences in the activity of these constituents and pH in the solution from which the mineral

grows (Hager et al. 2009). Anyway, our data clearly show that sulfur is dominant within the structure. The sulfur content of the examined samples is close to other data reported for cyanotrichite (e.g., Palache et al. 1951; Ankinovich et al. 1963), pointing to a completely carbonate-free cyanotrichite. Accordingly, the FTIR spectrum (Fig. 3) shows no peaks in the region of the C–O stretching band around 1400 cm^{−1}.

The FTIR spectrum (Fig. 3) displays a broadband due to OH stretching from 3800 to 2500 cm^{−1} with a peak at 3216 cm^{−1} and shoulders at 3340 and 2940 cm^{−1}. The

Fig. 3 FTIR infrared spectrum of cyanotrichite from Dachang deposit in the MIR region from 4000 to 400 cm^{-1}



absorption band at 1650 cm^{-1} is due to H–O–H bending, indicating the presence of water. The spectrum in the low-frequency 1300–480 cm^{-1} range is dominated by the absorption of the S–O bonds. Our data are in agreement with the FTIR data reported for analogous cyanotrichite samples (i.e., Chukanov et al. 1999; Hager et al. 2009).

On the basis of previous literature on similar compounds (e.g., Ross 1974; Lane 2007), the most intense bands at 1104 and 1037, with an additional shoulder at 1137 cm^{-1} , are due to stretching vibrations (ν_3) of the $(\text{SO}_4)^{2-}$ group. The antisymmetric bending modes (ν_4) are located at 660, 609 and 577 cm^{-1} , while the band at 507 cm^{-1} can be assigned to the ν_2 $(\text{SO}_4)^{2-}$ mode. The position of the hydroxyl stretching vibration can be used to estimate the hydrogen bond distances, $\text{O}_{\text{donor}} \cdots \text{O}_{\text{acceptor}}$ in linear OH \cdots O system through a correlation curve established by Libowitzky (1999). Accordingly, the frequencies measured for the examined cyanotrichite can be assigned to the presence of medium-strong H bonds in the structure characterized by $\text{O}_{\text{donor}} \cdots \text{O}_{\text{acceptor}}$ bond lengths varying in the range 2.64–2.76 Å.

Cell determination of cyanotrichite by ADT and synchrotron XRPD

Three-dimensional ADT data taken from different nano-sized cyanotrichite fragments reveal the occurrence of two different monoclinic phases. Energy-dispersive X-ray analysis performed on several spots of each phase showed similar content of Cu, Al and S. No fluorine was detected. These two phases are compositionally undistinguishable within the accuracy of the TEM–EDS analysis, which could correspond to two different polymorphic modifications, and have similar unit-cell parameters, clearly distinguishable

only by the values of the β angle: $a = 12.4(2)$, $b = 2.94(6)$, $c = 10.1(2)$ Å, $\beta = 98.6(5)^\circ$ and $a = 12.3(2)$ Å, $b = 2.94(6)$ Å, $c = 10.0(2)$ Å and $\beta = 92.2(5)^\circ$, hereafter labeled as cyanotrichite-98 and cyanotrichite-92, respectively. For both of them, systematic absences pointed to $C2/m$, $C2$ or Cm as possible space groups. It should be noted, however, that no evidence of such different phases could be detected during conventional TEM analyses. As a matter of fact, the morphology of the crystals (flattened on (001) and elongated along **b**), as well as the commensurability of the two phases and their iso-orientation along c^* , prevents TEM observations along the most informative observation direction for the measurement of beta angles.

Overall, five different crystals were investigated with ADT. Among them, one showed a diffuse scattering along c^* direction and numerous reflections from other crystallites with different orientations, so preventing any cell determination, three (Fig. 4a, b) showed solely the phase with $\beta \approx 98^\circ$ (cyanotrichite-98), and one produced two sets of reflections that could be completely indexed only superimposing the two cells reported above (Fig. 4c, d). The possibility of a twinning operation as the cause of the peak splitting was checked and discarded. Completeness and the R_{sym} of the datasets for the phase cyanotrichite-98 were (Dataset#1) R_{sym} 26.19 % Compl 42 %; (Dataset#2) R_{sym} 14.86 % Compl 44 %; (Dataset#3) R_{sym} 17.25 % Compl 65 %.

Taking into account the ADT results, the X-ray powder pattern could be fully described only by considering both the two cyanotrichite-like phases (Fig. 5). The Le Bail refinement of XRPD data, performed starting from cell parameters obtained by ADT, gives the following cell parameters: (1) $a = 12.417(2)$ Å, $b = 2.907(1)$ Å, $c = 10.157(1)$ Å and $\beta = 98.12(1)^\circ$; (2) $a = 12.660(2)$ Å, $b = 2.897(1)$ Å, $c = 10.162(1)$ Å and $\beta = 92.42(1)^\circ$.

Fig. 4 ADT reconstructed 3D diffraction volume of cyanotrichite. Diffraction volume of an ordered cyanotrichite-98 domain viewed along c^* (a) and along b^* (b). Diffraction volume of a mixed cyanotrichite-98 and cyanotrichite-92 domain viewed along c^* (c) and along b^* (d). In order to simplify the visualization in d, small differences in a^* and b^* directions for cyanotrichite-98 and cyanotrichite-92 are not shown. Few reflections that cannot be indexed by the displayed cells belong to another crystal, possibly a cyanotrichite-98 domain with different orientations

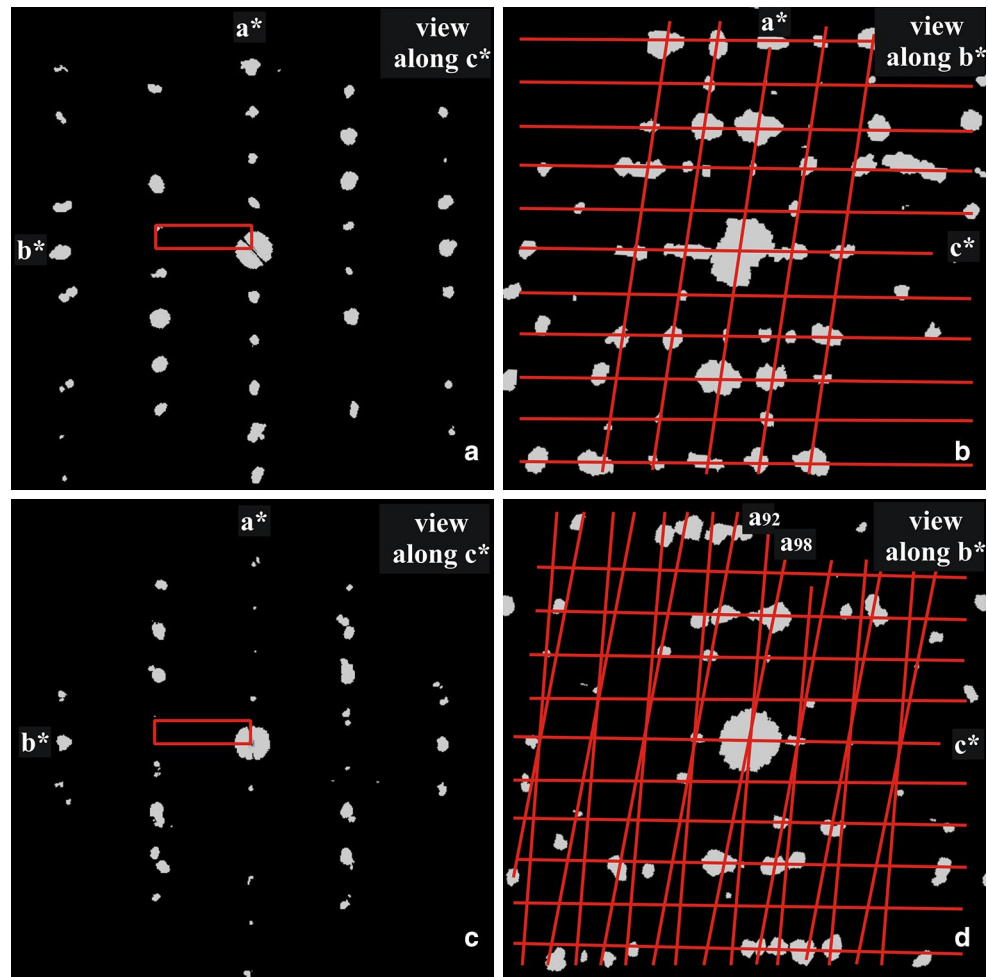
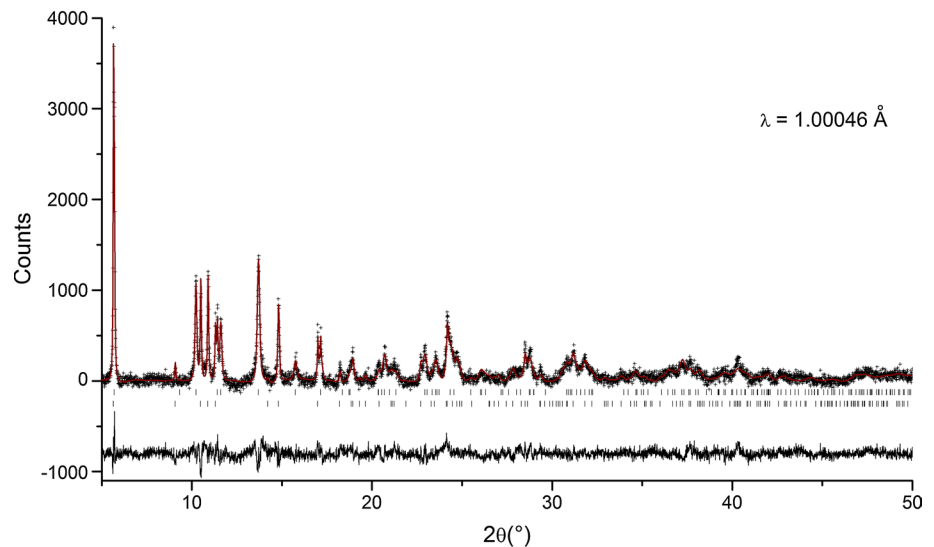


Fig. 5 Le Bail refinement plot for the cyanotrichite from Dachang deposit. The crosses represent the observed X-ray powder data points and the smooth red line through them the calculated pattern using GSAS. The first and second row of vertical tick marks represent Bragg positions of the cyanotrichite-92 and cyanotrichite-98 phase, respectively. The graph at the bottom is the residue between the experimental and the calculated pattern



The cyanotrichite-98 structure model on the basis of ADT data

An ab initio structure determination on the basis of ADT data was only possible for cyanotrichite-98 since the

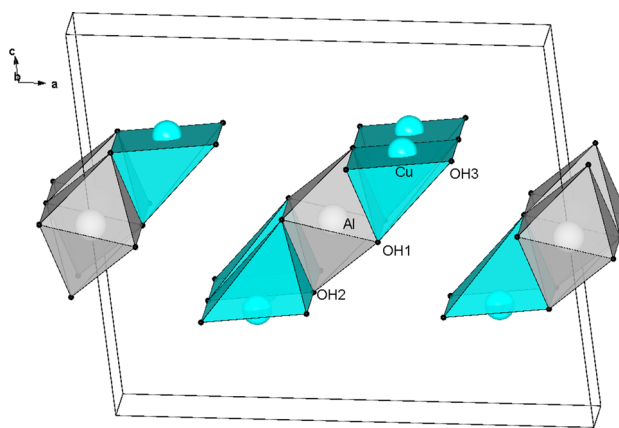
unique dataset available for cyanotrichite-92 revealed of insufficient quality for the structure determination. Direct methods as implemented in the SIR2011 program (Burla et al. 2012) allowed to solve the structure in the centro-symmetric $C2/m$ space group. However, similar

Table 2 Refined coordinates and equivalent isotropic displacement parameters (\AA^2) of atoms of main block in cyanotrichite-98 as determined by direct methods in space group $C2/m$

Atom	x/a	y/b	z/c	$U_{\text{iso/eq}}$
Al	0.5000	0.5000	0.5000	0.081 (5)
Cu	0.8269 (7)	0.5000	0.2832 (14)	0.072 (8)
OH1	0.9059 (13)	0.5000	0.5196 (17)	0.044 (5)
OH2	0.4366 (13)	0.5000	0.3134 (11)	0.044 (5)
OH3	0.7218 (12)	0.0000	0.2675 (33)	0.050 (6)

results were also obtained in the space groups $C2$ and Cm . Three independent solutions were achieved using intensities integrated from the three datasets showing solely cyanotrichite-98 reflections. The best dataset for structure solution and refinement was acquired with a cryo-holder at 155 K. Completeness and data quality are limited by the beam sensitivity of the material, connected with the important amount of structural water, and the fact that with a cryo-sample holder, the tilt range is reduced. The best trial solution showed an R value of about 27 % and an overall atom displacement parameter U of 0.028 \AA^2 . All solutions were very similar regarding the positions of one Al, one Cu and three O independent atoms (Table 2). The missing O and S atoms were tentatively searched in the difference Fourier map, calculated after few cycles of least-squares refinement. Although some positive peaks of residual electron density could be ascribed to water molecule and sulfur, these positions appeared unstable during refinement, probably because of the low electron density related to positional disorder. Overall, the data were sufficient to show the relevant topological and geometrical features of the main building block of the structure, allowing to build a reasonable structural model for cyanotrichite-98.

The main building block of the structure contains an Al site coordinated by six OH^- groups in a distorted octahedral arrangement, with four short Al–OH1 bonds (1.89 \AA) that define the corners of an equatorial square, and two slightly longer (1.95 \AA), symmetrically related Al–OH2 bonds that define the apexes of the octahedron (Fig. 6). Each Al octahedron shares two opposite equatorial edges with adjacent $[\text{Al}(\text{OH})_6]^{3-}$ octahedra, forming a column running along \mathbf{b} , while the other four edges, involving the apical OH^- groups, are shared with two symmetrically related Cu polyhedra. The Cu site exhibits a nearly square planar coordination with four Cu– OH^- distances between 1.95 (Cu–OH3) and 1.99 \AA (Cu–OH2) and forms a longer bond length (2.46 \AA) with another hydroxyl group (OH1). As required by the stoichiometry, an H_2O molecule (labeled Ow), with 0.5 occupancy, has been added to complete the sixfold coordination around Cu. Such distorted $(4 + 2)$ octahedral arrangement is due to the Jahn–Teller

**Fig. 6** Partial structural unit of cyanotrichite-98, obtained from direct methods in space group $C2/m$, drawn approximately along \mathbf{b}

effect (Jahn and Teller 1937) affecting the Cu^{2+} cations and is present also in khaidarkanite (Rastsvetaeva et al. 1997), and more in general, it is known to be typical of Cu^{2+} oxy-salts (Burns and Hawthorne 1996). A direct consequence of the half occupancy of the water group is that the mirror plane is only a statistical mirror, i.e., a mirror present only in the average structure, not locally. A similar situation occurs also in the structure of khaidarkanite in which a mirror plane arises from the statistical mixing of a hydroxyl group and a water molecule. Overall, the Cu octahedra form a column parallel to \mathbf{b} by sharing two opposite short edges. Together, Al- and Cu columns interact to form three polyhedra wide ribbons lying on $(1\ 0\ -1)$ and running along \mathbf{b} . The connection between these ribbons is achieved by hydrogen bonding involving OH1, and via SO_4^{2-} tetrahedra and water molecules, as discussed forward.

Completion of the model

Cyanotrichite-98 can be considered as being analogous to khaidarkanite with SO_4 replacing AlF_3 . This situation has been considered and elaborated in our model refining the best arrangement of the SO_4^{2-} group via geometric and charge-balance considerations. Possible orientations of this group has been tested assuming S–O average distances from literature data concerning hydrated sulfates, i.e., following Palmer et al. (1972) and Hawthorne et al. (2000). Upon this condition, a tetrahedral oxygen atom linked to a central S^{6+} cation receives from this, on average, about 1.50 v.u. and must receive additionally about 0.50 v.u. from another cation, so that bond-valence requirements could be satisfied. This condition is commonly achieved in minerals either when the oxygen is bonded to an additional di- or trivalent octahedrally (or higher) coordinated cation or when the oxygen atom acts as a hydrogen-bond acceptor. As a matter of fact, in the partial structure derived by

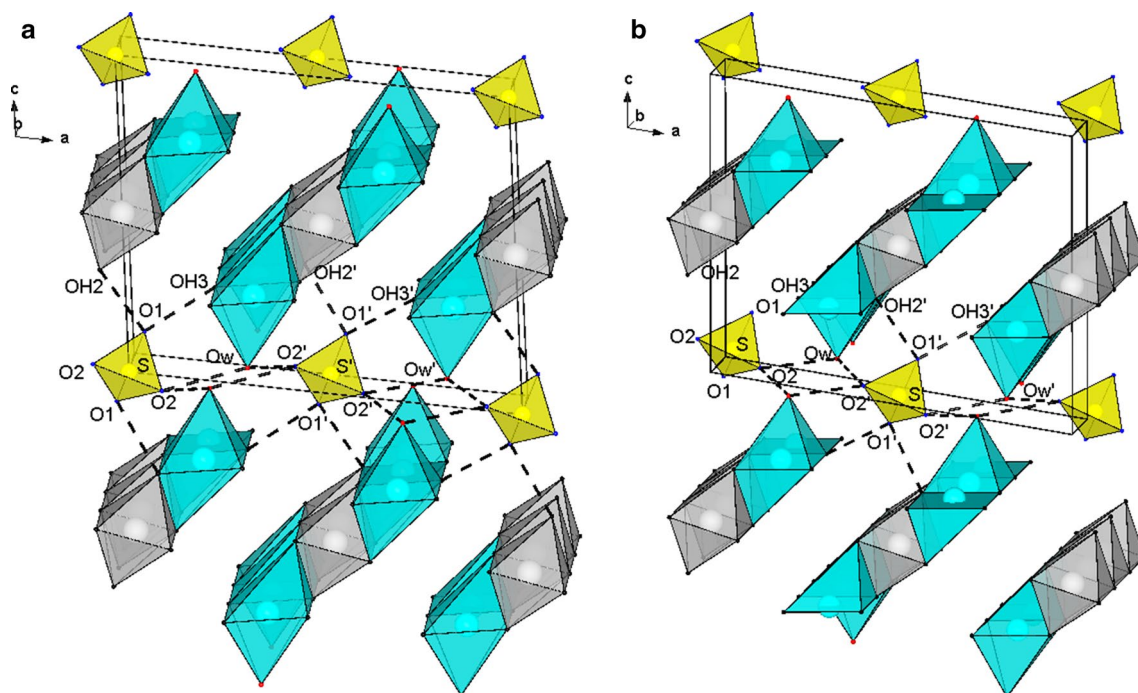


Fig. 7 Sketch of structural model for cyanotrichite-98 showing hydrogen bonds between SO_4 groups and hydroxyl groups and water molecules of the main structural units. **a** With SO_4 groups at special site 0,0,0 and $1/2,1,0$. **b** With SO_4 groups translated by $\mathbf{b}/2$

electron diffraction data, only if sulfate groups are located at 0, y , 0 and $1/2$, y , 0, two symmetrically related apices (labeled O1 and O1') can receive contributions from hydrogen belonging to hydroxyl group OH2 and OH3, as shown in Fig. 7. In such a case, the distance between the S and Cu sites excludes the possibility that the sulfate group could share two apical tetrahedral oxygens with the Cu octahedra. Additionally, if the sulfate groups are placed right at the special positions 0,0,0, and $1/2,1,0$ (or at $0,1/2,0$ and $1/2,3/2,0$), the two apical tetrahedral oxygens (labeled O2 and O2') can be involved in hydrogen-bond contributions from water molecules of Cu octahedra belonging to two adjacent chains (Fig. 7a, b).

Structural constraints suggest only two possible local arrangements of sulfate group and water molecule, separated by a translation vector $\mathbf{b}/2$, to complete properly the model. If the sulfate group and the water molecule are placed in one of these possible positions, the local symmetry is lowered down to $P2$. Although the periodic structure formed by one of these local ordered arrangements would have symmetry $P2$, the average structure, arising from the statistical positional disorder of sulfate group and water molecule, has symmetry $C2/m$ (Fig. 8) in agreement with the C -centering symmetry observed in the diffraction pattern.

Following Ferraris and Ivaldi (1988), the positions of the oxygens of the sulfate group and of the water

molecule were optimized to achieve the best possible hydrogen-bond scheme around the sulfate group for the $\text{O}_{\text{donor}} \cdots \text{O}_{\text{acceptor}}$ distances involved. The derived atomic coordinates for one of these local arrangements are reported in Table 3. In this optimized arrangement, we found the following $\text{O}_{\text{donor}} \cdots \text{O}_{\text{acceptor}}$ distances and valence units (v.u.): $\text{OH2} \cdots \text{O1} = 2.60 \text{ \AA}$ (0.29 v.u.); $\text{OH3} \cdots \text{O1} = 2.70 \text{ \AA}$ (0.23 v.u.); $\text{Ow} \cdots \text{O2} = 2.77 \text{ \AA}$ (0.20 v.u.); $\text{Ow}' \cdots \text{O2} = 2.78 \text{ \AA}$ (0.19 v.u), which result in valence sums close to the expected oxygen value (2.00 v.u), once taken into account the contributions of the oxygens belonging to sulfate group: $\text{S-O1} = 1.48 \text{ \AA}$ (1.48 v.u.); $\text{S-O2} = 1.45 \text{ \AA}$ (1.60 v.u).

As quoted above, in order to fulfill the stoichiometry requirements, the occupancy of the sulfate group and water molecule sites must be halved. This entails SO_4^{2-} groups and the water molecules with full occupancies alternating along [010] with vacant sites, doubling the \mathbf{b} periodicity in case of perfect order. As a consequence, at vacant sites, the Cu cation should result in a fivefold coordination. We observe that the halved occupancy of SO_4^{2-} group and of the water molecule joined to the disordering of these arrangements over the two positions translated by $\mathbf{b}/2$ cause the consequent lowering and spreading of the electron density that would explain the missing of the SO_4^{2-} group and water molecule during the ab initio structure solution.

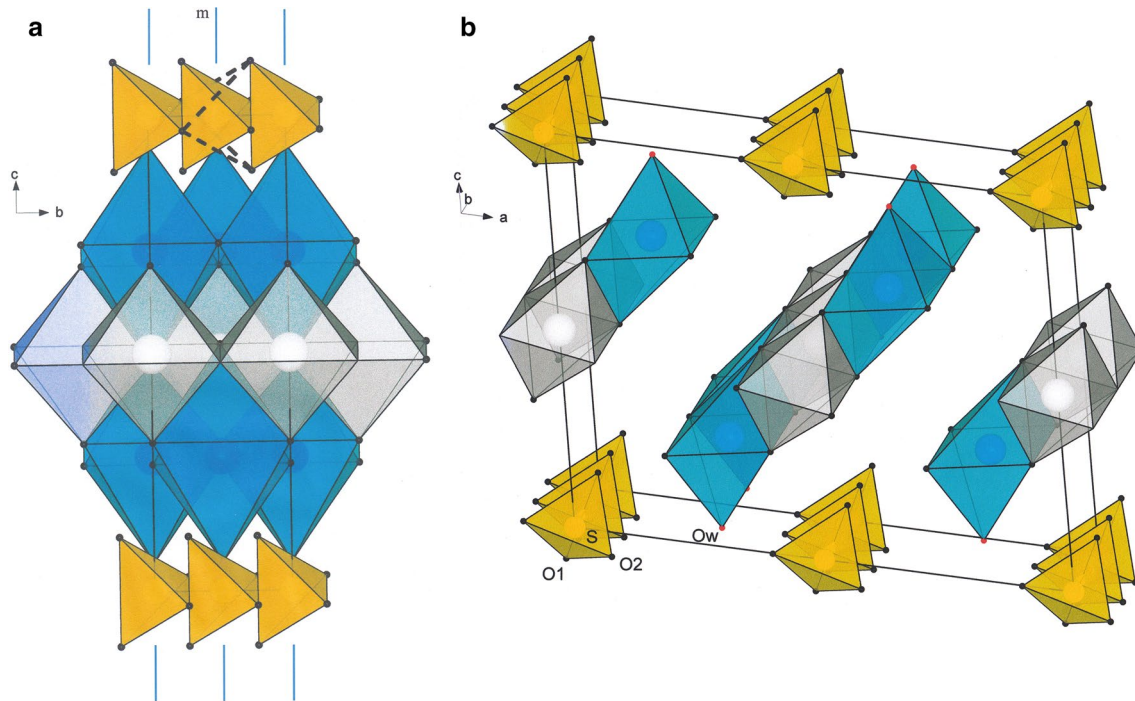


Fig. 8 The average structure of cyanotrichite-98 in space group $C2/m$ projected along $[100]$ (a) and along $[010]$ (b). For sake of clarity, only one mirror related SO_4 tetrahedra is dotted (a). The SO_4 group and the water molecule O_w have halved occupancy

Table 3 Atomic coordinates for structural model proposed for cyanotrichite-98 in space group $P2$

Atom	x/a	y/b	z/c	Atom	x/a	y/b	z/c
Al1	0.0000	0.0000	0.5000	Al2	0.5000	0.5000	0.5000
Cu1	0.3269	0.5000	0.2832	Cu2	0.8269	0.5000	0.2832
OH1	0.5942	0.0000	0.4804	OH1'	0.0942	0.5000	0.4804
OH2	0.4366	0.5000	0.3134	OH2'	0.9366	0.0000	0.3134
OH3	0.2218	0.5000	0.2675	OH3'	0.7218	0.0000	0.2675
O_w^a	0.3046	-0.1200	0.0610	$O_w'^a$	0.8040	0.5200	0.0560
S1	0.0000	0.5000	0.0000	S2	0.5000	0.5000	0.0000
$O1^a$	0.0414	0.2960	0.1151	$O2'^a$	0.5390	0.2960	0.1151
$O2^a$	0.0866	0.7020	-0.0325	$O1'^a$	0.5866	0.7020	-0.0309

^a Determined by geometric and charge-balance considerations

Related minerals

Cyanotrichite is related to khaidarkanite, $Cu_4Al_3(OH)_{10}F_3 \cdot 2H_2O$ (Rastsvetaeva et al. 1997), carbonate-cyanotrichite, ideally $Cu_4Al_2CO_3(OH)_{12} \cdot 2H_2O$ (Ankinovich et al. 1963), and camerolaeite, $Cu_4Al_2[HSbO_4, SO_4](OH)_{10}(CO_3) \cdot 2H_2O$ (Sarp and Perroud 1991). According to our model, the cyanotrichite-98 is based on a main block consisting of a central Al octahedron connected by edge-sharing to two adjacent distorted Cu polyhedra. The principal block of cyanotrichite-98 presented in this study is identical to that of khaidarkanite (Fig. 9). This is in agreement with Hager et al. (2009), who predicted a close relationship

between the cyanotrichite and khaidarkanite structures. The principal difference between the two structures involves the linkage of the ribbon-like units along the c direction. In khaidarkanite, columns of edge-sharing octahedral of composition $[AlF_4(H_2O, OH)_2]_{0.5}$ bridge adjacent ribbon-like units by sharing the H_2O groups with Cu polyhedra. In the cyanotrichite-98 model, the (SO_4) tetrahedra replaces $[AlF_4(H_2O, OH)_2]$ octahedra and the linkage between the ribbon-like units along $[001]$ occurs via hydrogen bonds between sulfate oxygens and water molecules belonging to the Cu octahedra.

The unit-cell parameters of cyanotrichite-98 are quite similar to those of khaidarkanite, as well as to those of

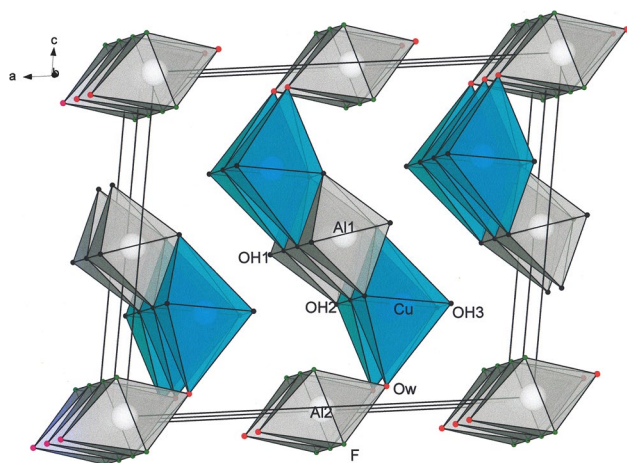


Fig. 9 The khaidarkanite structure viewed along [010]. The Al2 site has an occupancy of 50 %, and the F site has an occupancy of 75 %

carbonate-cyanotrichite, which is considered the carbonate analogue of cyanotrichite. All these structures are characterized by a unit cell with a beta angle of about 98° , whereas unit-cell parameters commonly reported for cyanotrichite are about 92° , thus analogous to the phase detected in this study and indicated as cyanotrichite-92. In spite of this similarity in unit-cell parameters, the lack of carbonate and the similar sulfur contents of cyanotrichite-98 and cyanotrichite-92 exclude the possibility that our cyanotrichite-98 could correspond to carbonate-cyanotrichite.

The crystal structure of carbonate-cyanotrichite is still unknown to date. However, the possibility of a carbonate-free structure related to carbonate-cyanotrichite has been hypostasized by Hager et al. (2009). Furthermore, Walenta (2001) reports a carbonate-free, cyanotrichite-like phase whose powder pattern could be indexed on a basis of a khaidarkanite unit cell. This structure results quite similar to the cyanotrichite-98 phase analyzed in this study.

Although the structure camerolaite is unknown so far, it is believed to be chemically and crystallographically related to cyanotrichite (Sarp and Perroud 1991). It is characterized by the substitution of most of SO_4 with HSbO_4 and the incorporation of a carbonate anion. It shows a monoclinic unit cell closely related to that of the other phases of the cyanotrichite group, with a beta angle of about 95° .

All the members of the cyanotrichite group share the same structural unit with composition $[\text{Cu}_4\text{Al}_2(\text{OH})_{12}]$, but differ by the presence of chemical species such as Al, S, Sb and C making anionic groups lying on the (001) plane. This explains the similar unit-cell parameters, as well as the possibility to index their powder diffraction pattern either by a *P* or *C* monoclinic unit cell. In fact, since the main structural unit $[\text{Cu}_4\text{Al}_2(\text{OH})_{12}]$ exhibits $C2/m$ symmetry, the occurrence of order or disorder of the Al, S, Sb and

C anionic groups in each respective structure can lead to apparent *P* or *C* unit cell, respectively (Hager et al. 2009).

Conclusions

The sample from Dachang deposit investigated in this study by means of automated electron diffraction tomography and synchrotron X-ray powder diffraction revealed of two distinct cyanotrichite-like phases, labeled cyanotrichite-98 and cyanotrichite-92, with metrically related monoclinic cells. These two phases resulted compositionally indistinguishable within the accuracy of TEM-EDS analysis. Infrared spectra do not evidence the presence of carbonate group in the structure. Only the cyanotrichite-98 phase was partially solved ab initio using ADT/PED data from individual nanosized domains. This partial structure, verified on the basis of three independent ADT/PED datasets, consists of a ribbon-like unit built with composition $[\text{Cu}_4\text{Al}_2(\text{OH})_{12}^{2+}]$. The remaining parts of the structure, namely the positions of the missing water molecule and the SO_4^{2-} anion, were deduced via geometric and charge-balance considerations. Structural constraints suggest two possible local arrangements, in *P2* symmetry, of water molecule and the SO_4^{2-} anion. The average structure arising from this statistical positional disorder shows the *C*-centering symmetry in agreement with ADT results.

Acknowledgments We thank Ute Kolb (University of Mainz) for technical support in ADT experiments. The authors are grateful to Stefano Merlini for constructive discussion. We thank two anonymous reviewers for their helpful suggestions. Funding for this study was provided through the Italian project FIR2013 “Exploring the nanoworld.”

References

- Ankinovich EA, Gekht II, Zaitseva RI (1963) A new variety of cyanotrichite—carbonate-cyanotrichite. *Zap Vser Miner Obshchest* 92:458–463 (in Russ.)
- Burla MC, Caliandro R, Camalli M, Carrozzini B, Cascarano G, Giacovazzo C, Mazzone A, Polidori G, Spagna R (2012) SIR2011: a new package for crystal structure determination and refinement. *J Appl Crystallogr* 45:357–361
- Burns PC, Hawthorne FC (1996) Static and dynamic Jahn–Teller effects in Cu^{2+} oxysalts. *Can Miner* 33:633–639
- Capitani GC, Oleynikov P, Hovmoeller S, Mellini M (2006) A practical method to detect and correct for lens distortion in the TEM. *Ultramicroscopy* 106:66–74
- Capitani GC, Mugnaioli E, Rius J, Gentile P, Catelani T, Lucotti A, Kolb U (2014) The Bi sulfates from the Alfenza Mine, Crodo, Italy: an automatic electron diffraction tomography (ADT) study. *Am Miner* 99:500–510
- Chukanov NV, Karpenko VY, Rastsvetaeva RK, Zadov AE, Kuz'mina OV (1999) Khaidarkanite $\text{Cu}_4\text{Al}_3(\text{OH})_{14}\text{F}_3 \cdot 2\text{H}_2\text{O}$, a new mineral from the Khaidarkan deposit, Kyrgyzstan. *Zap Vser Miner Obshchest* 128(3):58–63 (in Russ.)

- Doyle P, Turner P (1968) Relativistic Hartree–Fock X-ray and electron scattering factors. *Acta Cryst A* 24:390–397
- Ferraris G, Ivaldi G (1988) Bond valence vs bond length in O...O hydrogen bonds. *Acta Cryst B* 44:341–344
- Gemmi M, Fischer J, Merlini M, Poli S, Fumagalli P, Mugnaioli E, Kolb U (2011) A new hydrous Al-bearing pyroxene as a water carrier in subduction zones. *Earth Planet Sci Lett* 310:422–428
- Hager SL, Leverett P, Williams PA (2009) Possible structural and chemical relationships in the cyanotrichite group. *Can Miner* 47:635–648
- Hawthorne FC, Krivovichev SV, Burns PC (2000) The crystal chemistry of sulfate minerals. In: Alpers CN, Jambor JL, Nordstrom BK (eds) *Sulfate minerals: crystallography, geochemistry, and environmental significance*. *Rev. Mineral. Geochem* 40 pp 1–112
- Jahn HA, Teller E (1937) Stability of polyatomic molecules in degenerate electronic states. *Proc R Soc Ser A* 161:220–236
- Jiang J, Jorda JL, Yu J, Baumes LA, Mugnaioli E, Diaz-Cabanias MJ, Kolb U, Corma A (2011) Synthesis and structure determination of the hierarchical meso-microporous zeolite ITQ-43. *Science* 333:1131–1134
- Kolb U, Gorelik TE, Kübel C, Otten MT, Hubert D (2007) Towards automated diffraction tomography: Part I—data acquisition. *Ultramicroscopy* 107:507–513
- Kolb U, Gorelik TE, Otten MT (2008) Towards automated diffraction tomography. Part II—cell parameter determination. *Ultramicroscopy* 108:763
- Kolb U, Gorelik TE, Mugnaioli E, Stewart A (2010) Structural characterization of organics using manual and automated electron diffraction. *Polym Rev* 50:385–409
- Kolb U, Mugnaioli E, Gorelik TE (2011) Automated electron diffraction tomography—a new tool for nano crystal structure analysis. *Cryst Res Technol* 46:542–554
- Lane MD (2007) Mid-infrared emission spectroscopy of sulfate and sulfate-bearing minerals. *Am Miner* 92:1–18
- Larson AC, Von Dreele RB (2000) General structure analysis system (GSAS). Los Alamos National Laboratory report LAUR 86–748
- Lausi A, Busetto E, Leoni M, Scardi P (2006) The MCX project: a Powder Diffraction beamline at ELETTRA. *Synchrotron Radiat Nat Sci* 5:1–2
- Libowitzky E (1999) Correlation of O–H stretching frequencies and O–H...O hydrogen bond lengths in minerals. *Monatsh Chem* 130:1047–1059
- Mason B (1961) The identity of namaqualite with cyanotrichite. *Mineral Mag* 32:737–738
- Mugnaioli E, Kolb U (2013) Applications of automated diffraction tomography (ADT) on nanocrystalline porous materials. *Microporous Mesoporous Mater* 166:93–101
- Mugnaioli E, Gorelik T, Kolb U (2009a) “Ab initio” structure solution from electron diffraction data obtained by a combination of automated diffraction tomography and precession technique. *Ultramicroscopy* 109:758–765
- Mugnaioli E, Capitani GC, Nieto F, Mellini M (2009b) Accurate and precise lattice parameters by selected area electron diffraction in the transmission electron microscope. *Am Miner* 94:793–800
- Mugnaioli E, Andrusenko I, Schüler T, Loges N, Dinnebier RE, Panthöfer M, Tremel W, Kolb U (2012) Ab initio structure determination of vaterite by automated electron diffraction. *Angew Chem Int Ed Engl* 51:7041–7045
- NanoMEGAS (2004) Advanced Tools for Electron Diffraction. <http://www.nanomegas.com>
- Palache C, Berman H, Frondel C (1951) *The system of mineralogy II*, 7th edn. Wiley, New York, pp 578–579
- Palmer KJ, Wong RY, Lee KS (1972) The crystal structure of ferric ammonium sulfate trihydrate, $\text{FeNH}_4(\text{SO}_4)_2 \cdot 3\text{H}_2\text{O}$. *Acta Cryst B* 28:236–241
- Percy J (1850) Chemical examination of letsomite. *Phil Mag Ser* 3(36):100–103
- Rastsvetaeva RK, Chukanov NV, Karpenko VU (1997) The crystal structure of a new compound $\text{Cu}_4\text{Al}_3(\text{OH})_{14}\text{F}_3(\text{H}_2\text{O})_2$. *Dokl Akad Nauk* 353:354–357
- Ross SD (1974) Sulphates and other oxy-anions of group VI. In: Farmer VC (ed) *The infrared spectra of minerals*. Mineralogical Society, London, pp 423–444
- Rozhdestvenskaya I, Mugnaioli E, Czank M, Depmeier W, Kolb U, Reinholdt A, Weirich T (2010) The structure of charoite, $(\text{K}, \text{Sr}, \text{Ba}, \text{Mn})_{15-16}(\text{Ca}, \text{Na})_{32}[(\text{Si}70(\text{O}, \text{OH})180)](\text{OH}, \text{F})_{4.0-n}\text{H}_2\text{O}$, solved by conventional and automated electron diffraction. *Mineral Mag* 74:159–177
- Rozhdestvenskaya I, Mugnaioli E, Czank M, Depmeier W, Kolb U, Merlino S (2011) Essential features of the polytypic charoite-96 structure compared to charoite-90. *Mineral Mag* 75:2833–2846
- Sarp H, Perroud P (1991) Camerolaite, $\text{Cu}_4\text{Al}_2[\text{HSbO}_4, \text{SO}_4](\text{OH})_{10}(\text{CO}_3) \cdot 2\text{H}_2\text{O}$, a new mineral from Cap Garonne mine, Var, France. *Neues Jahrb Miner Monatsh* 2:481–486
- Sheldrick GM (1997) SHELXL97: program for the refinement of crystal structures. University of Göttingen, Göttingen
- Vincent R, Midgley P (1994) Double conical beam-rocking system for measurement of integrated electron diffraction intensities. *Ultramicroscopy* 53:271–282
- Walenta K (2001) Ein cyanotrichitähnliches Mineral von der Grube Clara. *Erzgräber* 15:29–35
- Werner AG (1808): *Mineralogische tabellen*. In: Karsten DLG, Rottman (eds) 2nd edn., Berlin, Germany, p 62